An unscented Kalman filter based navigation algorithm for autonomous underwater vehicles

DOI 10.1016/j.mechatronics.2016.05.007

An Unscented Kalman Filter Based Navigation Algorithm for Autonomous Underwater Vehicles

B. Allotta[1,5], A. Caiti[3,5], L. Chisci[2], R. Costanzi[3,5], F. Di Corato[4], C. Fantacci[2], D. Fenucci[3,5], E. Meli[1,5], A. Ridolfi[1,5]

1 University of Florence - Department of Industrial Engineering (DIEF)
Via di Santa Marta 3, Florence, Italy. Email: a.ridolfi@unifi.it

2 University of Florence - Department of Information Engineering (DINFO)
Via di Santa Marta 3, Florence, Italy

3 University of Pisa - DII & Centro Piaggio
Largo Lucio Lazzarino 1, Pisa, Italy

4 Magneti Marelli S.p.A. ADAS Technologies, CTO, Venaria (TO), Italy
Work done when this author belonged to 3, 5

5 Interuniversity Center of Integrated Systems for the Marine Environment (ISME) - www.isme.unige.it

Abstract

Robust and performing navigation systems for Autonomous Underwater Vehicles (AUVs) play a discriminant role towards the success of complex underwater missions involving one or more AUVs. The quality of the filtering algorithm for the estimation of the AUV navigation state strongly affects the performance of the overall system. In this paper, the authors present a comparison between the Extended Kalman Filter (EKF) approach, classically used in the field of underwater robotics and an Unscented Kalman Filter (UKF). The comparison results to be significant as the two strategies of filtering are based on the same process and sensors models. The UKF-based approach, here adapted to the AUV case, demonstrates to be a good trade-off between estimation accuracy and computational load. *UKF has not yet been extensively used in practical underwater applications, even if it turns out to be quite promising.* The proposed results rely on the data acquired during a sea mission performed by one of the two Typhoon class vehicles involved in the NATO CommsNet13 experiment (held in September 2013). As ground truth for performance evaluation and comparison, performed offline, position measurements obtained through Ultra-Short BaseLine (USBL) fixes are used. The result analysis leads to identify both the strategies as effective for the purpose of being included in the control loop of an AUV. The UKF approach demonstrates higher performance encouraging its implementation as a more suitable navigation algorithm even if, up to now, it is still not used much in this field.

Keywords: Underwater Navigation, Autonomous Underwater Vehicles, Unscented Kalman Filter, Underwater Robotics

1. Introduction

Autonomous Underwater Vehicles (AUVs) are increasingly employed in underwater operations and are fundamental for many scientific and industrial tasks (e.g. Oil & Gas operations, exploration and surveillance of archeological sites, reconnaissance and patrolling for military operations and so on).
The development of accurate and robust navigation strategies for AUVs is crucial to reach the high control performance required by complex underwater missions involving one or more AUVs [19] [14] [32] [18]. More particularly, one of the main factors affecting the AUVs navigation accuracy is the algorithm used to estimate the vehicle motion. They are usually based on Kalman Filters (KF) [24] or Extended Kalman Filters (EKF) [11] [36] [27] [6] and make use of simplified kinematic or dynamic vehicle models .
Furthermore, different sets of sensors are employed during the vehicle navigation. They may include, for instance, Inertial Measurement Units (IMU) [10] [40] or Fiber Optic Gyros (FOG) [28] [4] to measure vehicle orientation, Pressure Sensors (PS) for depth measurements, Doppler Velocity Logs (DVL) [10] to measure the vehicle translational velocity, acoustic localization systems based on range measurements [9] [13] [31] [21] [15] or on Ultra-Short BaseLine (USBL) [26] [34] [37].
In this paper, the authors present a navigation system specifically designed for AUVs and its experimental evaluation in typical underwater missions. The developed system exploits inertial sensors, depth sensors and Global Positioning System

(GPS) fixes (during periodic resurfacing) and relies on the Unscented Kalman Filter (UKF) [23] [39] [35] for motion estimation. *The UKF-based approach, here adapted to the AUV case, demonstrates to be a good trade-off between estimation accuracy and computational load. However, to the authors' knowledge, it has not yet been largely used for underwater navigation in practical underwater tasks [22] [12] [25]. Up to know, previous results in literature related to the use of UKF in the underwater field are in almost all cases based on simulated data. On the contrary the here proposed results, for offline validation purposes, rely on the experimental data acquired during a sea mission* performed by one of the two Typhoon class vehicles involved in the NATO CommsNet13 experiment (held in September 2013). *The main contribution of the paper is related to the correct implementation of this filter, which is strictly related to the AUV modelling (including the correct modelling of the non-linear dynamics of this kind of system, e.g. the propulsion part) and in the experimental validation of the proposed approach.* As ground truth for performance evaluation and comparison, performed offline, position measurements obtained through Ultra-Short BaseLine (USBL) fixes are used. The sea tests were performed in La Spezia (Italy) with the Typhoon AUV (see Fig. 1, [2] [5]) in the framework of the Italian THESAURUS project [3] and the European ARROWS project [1] during the NATO CommsNet13 experiment, in September 2013. Typhoon is an AUV designed by the Department of Industrial Engineering (DIEF) of the Florence University for exploration and surveillance of underwater archaeological sites. Currently two versions of the Typhoon AUV have been built, characterized by different sensors and payloads. The vehicles are named TifOne and TifTu respectively. The test campaign described in this paper has been performed using the TifTu vehicle equipped with a sensor set including an IMU (with 3D accelerometer, gyroscope and magnetometer), a pressure sensor for the depth, GPS and USBL.

The experimental measurements taken with TifTu include the

Figure 1: The Typhoon AUV during the sea tests in La Spezia (Italy).

sensor data concerning the vehicle dynamics (IMU and pressure sensor), global positioning system (GPS) fixes obtained through periodic and dedicated vehicle resurfacing [41] [29] and global positioning provided by the USBL and obtained thanks to the permanent testbed for underwater networking and communication purposes (LOON - Littoral Ocean Observatory Network) of the NATO Science and Technology Organization Centre for Maritime Research and Experimentation (NATO STO CMRE) [8]. The USBL fixes are not exploited by the navigation system, being only used as a reference (ground truth) to evaluate the algorithm accuracy.

At this initial stage of the research activity, the experimental underwater test has been performed with the AUV autonomously navigating in dead reckoning along a triangle-shaped path. To effectively evaluate the navigation system performance, the validation has been performed offline, applying the new navigation system to experimental data measured on the vehicle navigating in dead reckoning.

A performance comparison between the proposed UKF-based navigation system and a standard EKF-based system [6] has been carried out. The comparison allowed the authors to evaluate the accuracy of the proposed navigation approach (very suitable for AUV navigation and, up to now, still not used much in this field) in estimating the vehicle dynamic behaviour without increasing the computational load (affordable for on-line on-board AUV implementation). The achieved results are encouraging, waiting for future online tests with the vehicle (both in simulation and during experimental campaigns).

2. General architecture

As pointed out in the introduction, the Typhoon AUV, thanks to its reconfigurability, allows to easily and effectively test the performance of different navigation algorithms. The typical test architecture is schematized in Fig. 2.

The Typhoon AUV navigates in dead reckoning using the

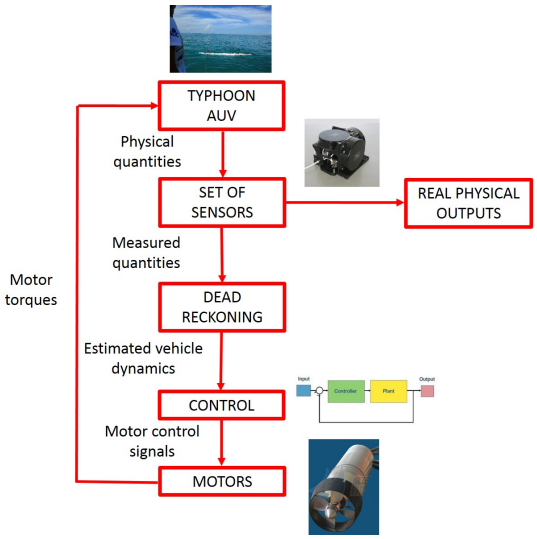

Figure 2: Online testing of navigation systems.

information coming from the available sensors. The physical quantities characterizing the Typhoon AUV dynamics (orientation, depth and position) are measured by the set of on-board sensors: IMU, pressure sensor, GPS (during periodic resurfacing) and USBL. Recall that the USBL is not exploited by

the navigation system, being only used as external reference to evaluate the localization accuracy. The measured quantities are then processed in dead reckoning to approximately estimate the vehicle dynamics. Starting from the estimated vehicle dynamics, the control is able to calculate the motor control signals [6]. Finally, the thrusts produced by the motors allow the vehicle to follow the desired dynamics.
The sensor suite provides the real physical outputs to be used to test and compare the different navigation systems (i.e., the EKF-based and UKF-based ones). The preliminary validation and analysis of the navigation system presented by the authors in this work are performed offline. The adopted architecture for offline testing is depicted in Fig. 3.
The test of the navigation system relies on the data measured

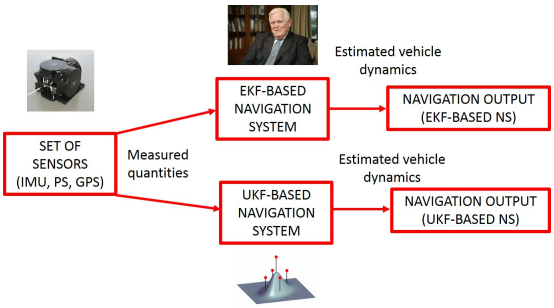

Figure 3: Offline testing of navigation systems.

by the sensor suite (IMU, pressure sensor and GPS during periodic resurfacing). The measured quantities (orientation, depth and position) are processed by both EKF and UKF algorithms in order to recursively generate estimates of the AUV state. Then, such estimates are compared to the USBL position fixes during the whole mission. In the sequel, the main parts of the proposed navigation system will be analyzed in detail. Then, an experimental evaluation of the navigation algorithm performance will follow.

3. The Typhoon AUV

In this chapter, the main parts of the Typhoon AUV architecture for the testing of navigation systems are described. The overall architecture is made up of the Typhoon AUV (navigating in dead reckoning), the set of sensors, the control logic and the propulsion system (motors). This general vehicle arrangement allows to get the real physical outputs necessary to effectively compare the EKF-based and UKF-based navigation systems (orientation, depth and GPS position during the resurfacing).

3.1. The vehicle

A new class of AUVs, called Typhoon, has been developed in the framework of the Italian THESAURUS project [3] and of the European ARROWS project [1], [7]. Typhoon is a middle-sized AUV able to reach a 300 $[m]$ depth. The vehicles can carry suitable payload for the specific underwater mission to perform. Currently, two Typhoon AUVs are fully operative and already performed many missions at sea: the vehicles are called TifOne and TifTu.
TifTu usually navigates both on surface and underwater and localizes itself though a GPS system (for the surface navigation) and an Ultra-Short BaseLine (USBL) acoustic system (for the underwater navigation). The USBL is a method of underwater acoustic localization based on the use of an acoustic transceiver (composed of a series of transducers) capable of communicating with a transponder. The adopted configuration involves a transceiver (the permanent LOON testbed placed on the seabed or a surface support vehicle) and a transponder (an acoustic modem) rigidly mounted on-board of the AUV navigating underwater.
TifTu, the AUV exploited during the CommsNet13 sea campaign, has a length of 3700 $[mm]$, an external diameter of 350 $[mm]$ and a weight of about 150 $[kg]$ according to the carried payload (the vehicle can be considered an intermediate one compared to the smaller Remus 100 [30] and the bigger Remus 600 [38]). Its autonomy is $8-10\,[h]$ and the maximum reachable longitudinal speed is 6 $[kn]$ (whereas the cruise speed is about 2 $[kn]$). The power needed by the propulsion onboard systems and payloads was approximately known (about 350 $[W]$): considering a mission duration of about $8-10\,[h]$, the needed energy was calculated in about $3-3.5\,[kWh]$. Li-Po (Lithium-Polymer) batteries have been chosen.
In Fig. 4, both the Typhoon CAD design and its final built versions can be seen.
The TifTu propulsion system is composed of 6 actuators: two

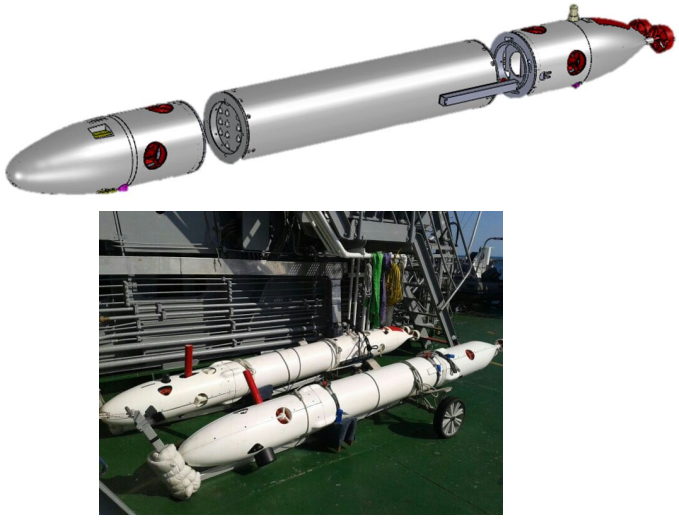

Figure 4: The Typhoon CAD design and its final built versions on the NATO Research Vessel Alliance during CommsNet13.

lateral thrusters, two vertical thrusters and two main rear propellers (both working in longitudinal direction). The propulsion system actively controls 5 Degrees Of Freedom (DOFs) of the vehicle (the only one left passive is the roll one). The correct positioning and alignment of the buoyancy and the gravity centers ensure the vehicle stability against roll motions. The calibration of the pitch can also be performed by moving the accumulators whose axial position is controlled by a screw sys-

tem.

3.1.1. Vehicle modelling

To analyze the motion of the AUV, two different reference frames are needed [19]:

- *the body frame*: reference frame with origin O^b placed in the center of mass of the body and axes lined up to the main inertia axes of the body itself. In case of a vehicle of regular shape, the x^b axis is longitudinal, pointing forward, the z^b axis is vertical downward and the y^b axis is set out in order to form a right-handed frame with the other two axes;

- *the fixed frame*: inertial reference frame, defined with the origin O^n placed on the surface and axes lined up to the ones of a NED (North-East-Down) frame. The x^n axis heads to the north, the y^n axis heads to the east and the z^n axis down.

To describe the motion of the system, the following coordinate vectors have to be introduced *(according to [20])*:

$$\boldsymbol{\eta} = \begin{pmatrix} \boldsymbol{\eta}_1 \\ \boldsymbol{\eta}_2 \end{pmatrix} = \begin{pmatrix} \boldsymbol{O}^b \\ \boldsymbol{\Phi} \end{pmatrix}, \qquad \boldsymbol{\nu} = \begin{pmatrix} \boldsymbol{\nu}_1 \\ \boldsymbol{\nu}_2 \end{pmatrix} = \begin{pmatrix} \dot{\boldsymbol{O}}^b \\ \boldsymbol{\omega}^b \end{pmatrix} \tag{1}$$

where $\boldsymbol{\eta}$ represents the vector of position $\boldsymbol{\eta}_1$ and orientation $\boldsymbol{\eta}_2$, *expressed in terms of the Roll-Pitch-Yaw (RPY) Euler angles (roll φ, pitch ϑ and yaw ψ)* in the fixed frame and $\boldsymbol{\nu}$ includes the components of linear $\boldsymbol{\nu}_1$ and angular $\boldsymbol{\nu}_2$ velocities expressed in the body frame.

$$\begin{array}{llll} \boldsymbol{\eta} = \left[\boldsymbol{\eta}_1^T \ \boldsymbol{\eta}_2^T\right]^T & \boldsymbol{\eta}_1 = [x\ y\ z]^T & \boldsymbol{\eta}_2 = [\varphi\ \vartheta\ \psi]^T \\ \boldsymbol{\nu} = \left[\boldsymbol{\nu}_1^T \ \boldsymbol{\nu}_2^T\right]^T & \boldsymbol{\nu}_1 = [u\ v\ w]^T & \boldsymbol{\nu}_2 = [p\ q\ r]^T \end{array} . \tag{2}$$

Clearly, the previous physical quantities are linked together by the following kinematic equations:

$$\begin{aligned} &\dot{\boldsymbol{\eta}} = J(\boldsymbol{\eta})\boldsymbol{\nu}, \\ &\begin{pmatrix} \dot{\boldsymbol{\eta}}_1 \\ \dot{\boldsymbol{\eta}}_2 \end{pmatrix} = \begin{bmatrix} J_1(\boldsymbol{\eta}_2) & 0_{3\times3} \\ 0_{3\times3} & J_2(\boldsymbol{\eta}_2) \end{bmatrix} \begin{pmatrix} \boldsymbol{\nu}_1 \\ \boldsymbol{\nu}_2 \end{pmatrix} = \\ &= \begin{bmatrix} R_b^n(\boldsymbol{\eta}_2) & 0_{3\times3} \\ 0_{3\times3} & T^{-1}(\boldsymbol{\eta}_2) \end{bmatrix} \begin{pmatrix} \boldsymbol{\nu}_1 \\ \boldsymbol{\nu}_2 \end{pmatrix} \end{aligned} \tag{3}$$

where R_b^n is the rotation matrix between the body and the fixed reference systems and T is the so called Euler matrix. Their explicit expressions are the following ones:

$$R_b^n(\boldsymbol{\eta}_2) = \begin{bmatrix} c\psi c\vartheta & -s\psi c\varphi + c\psi s\vartheta s\varphi & s\psi s\varphi + c\varphi s\vartheta c\psi \\ s\psi c\vartheta & c\psi c\varphi + s\psi s\vartheta s\varphi & -c\psi s\varphi + c\varphi s\vartheta s\psi \\ -s\vartheta & s\varphi c\vartheta & c\varphi c\vartheta \end{bmatrix}$$

$$T^{-1}(\boldsymbol{\eta}_2) = \begin{bmatrix} 1 & s\varphi t\vartheta & c\varphi t\vartheta \\ 0 & c\varphi & -s\varphi \\ 0 & s\varphi/c\vartheta & c\varphi/c\vartheta \end{bmatrix} \tag{4}$$

On the other hand, the motion of the AUV is governed by the vehicle dynamic equations:

$$M\dot{\boldsymbol{\nu}} + C(\boldsymbol{\nu})\boldsymbol{\nu} + D(\boldsymbol{\nu})\boldsymbol{\nu} + \boldsymbol{g}(\boldsymbol{\eta}) = \boldsymbol{\tau}(\boldsymbol{\nu}, \boldsymbol{u}) \tag{5}$$

where M is the mass matrix, C is the centrifugal and Coriolis matrix, D is the drag matrix, $\boldsymbol{g}$ is the gravity and buoyancy vector and $\boldsymbol{\tau}(\boldsymbol{\nu}, \boldsymbol{u})$ are the resultant forces and torques acting on the vehicle ($\boldsymbol{u}$ are the control signals of the vehicle motors, i. e. the motor rotation speeds). *The explicit expressions of all these physical quantities, not reported here for reasons of brevity, can be found in [19], [20].* It is worth to note that the vehicle dynamic equations (5) are non-linear with respect to the vehicle velocity. Moreover, the input vector τ depends upon the motor thrusts (please see paragraph 3.3.1 for details) that are highly non-linear and non-differentiable functions of the vehicle velocity (in particular of the axial velocity of each propeller) and of the rotational speed of each propeller. Introducing the state vector $\boldsymbol{x} = \begin{pmatrix} \boldsymbol{\nu}^T & \boldsymbol{\eta}^T \end{pmatrix}^T$, the system equations can be summarized as follows:

$$\begin{aligned} &\dot{\boldsymbol{x}} = \boldsymbol{F}(\boldsymbol{x}, \boldsymbol{u}) + \boldsymbol{w} = \\ &= \begin{pmatrix} M^{-1}\left[\boldsymbol{\tau}(\boldsymbol{\nu}, \boldsymbol{u}) - C(\boldsymbol{\nu})\boldsymbol{\nu} - D(\boldsymbol{\nu})\boldsymbol{\nu} - \boldsymbol{g}(\boldsymbol{\eta})\right] \\ J(\boldsymbol{\eta})\boldsymbol{\nu} \end{pmatrix} + \boldsymbol{w} \end{aligned} \tag{6}$$

where $\boldsymbol{w}$ is the process noise.

3.2. The sensors

Hereinafter, the set of on-board sensors employed during the navigation by the Typhoon AUV is briefly described:

- *IMU Xsens MTi*: the device consists of a 3D gyroscope, a 3D accelerometer and a 3D magnetometer providing measurements at a maximum working frequency of 100 $[Hz]$. The device estimates the orientation of the vehicle in a 3D space in an accurate way by means of an embedded attitude estimation algorithm;

- *STS DTM depth sensor*: it is a digital pressure sensor used to measure the vehicle depth at a 10 $[Hz]$ working frequency;

- *GPS*: the global positioning system is included into the industrial PC-104. This sensor, working at 1 $[Hz]$, is employed to get suitable fixes only during periodic and dedicated vehicle resurfacing;

- *USBL 18/34 by EvoLogics*: this sensor is not exploited by the navigation systems and is only used as an external benchmark to evaluate the algorithm accuracy. The sensor works at a maximum working frequency of 0.2 $[Hz]$. Actually, the real working frequency can be quite lower depending on the quality of the acoustic channel.

The sensor set here proposed is quite a standard one and not very expensive.

3.2.1. Sensors modelling

Hereafter, the measurement equations modelling the sensor behaviour will be derived by taking into account the main features of the employed sensors and the main noise sources affecting the measurements:

- *vehicle orientation* $\boldsymbol{\eta}_2$ provided by the IMU Xsens MTi (including 3D gyroscope, 3D accelerometer and 3D magnetometer) through the attitude estimation filter starting from the following measures:

  - *Vehicle angular velocity* $\boldsymbol{\nu}_2$ measured by the 3D gyroscope:
  $$\boldsymbol{\nu}_2^{meas} = \boldsymbol{\nu}_2 + \boldsymbol{\delta}_{\nu 2} \tag{7}$$
  where $\boldsymbol{\nu}_2^{meas}$ and $\boldsymbol{\nu}_2$ denote the measured *and the true* angular *velocities* and $\boldsymbol{\delta}_{\nu 2}$ is the measurement noise;

  - *Vehicle linear acceleration* measured by the 3D accelerometer:
  $$\boldsymbol{a}^{meas} = \boldsymbol{a} + \boldsymbol{\delta}_a \tag{8}$$
  where $\boldsymbol{a}^{meas}$ and $\boldsymbol{a}$ denote the measured *and the true* linear *accelerations* and $\boldsymbol{\delta}_a$ is the measurement noise;

  - *Magnetic field* $\boldsymbol{M}$ measured by the 3D magnetometer:
  $$\boldsymbol{M}^{meas} = \boldsymbol{M} + \boldsymbol{\delta}_M \tag{9}$$
  where $\boldsymbol{M}^{meas}$ and $\boldsymbol{M}$ denote the measured *and the true* magnetic *fields* and $\boldsymbol{\delta}_M$ is the measurement noise.

  By suitably processing the above measurements, the attitude estimation filter is able to estimate the vehicle orientation $\boldsymbol{\eta}_2$ that will be used in the subsequent developments of this paper as a virtual measurement $\boldsymbol{\eta}_2^{meas}$ modeled as:
  $$\boldsymbol{\eta}_2^{meas} = \boldsymbol{\eta}_2 + \boldsymbol{\delta}_{\eta 2} \tag{10}$$
  where $\boldsymbol{\delta}_{\eta 2}$ is a further measurement noise.

- *vehicle position* η_{1x} and η_{1y} measured by the GPS sensor:
$$\begin{aligned} \eta_{1x}^{meas} &= \eta_{1x} + \delta_x \\ \eta_{1y}^{meas} &= \eta_{1y} + \delta_y \end{aligned} \tag{11}$$
where η_{1x}^{meas}, η_{1y}^{meas} and η_{1x}, η_{1y} are the measured *and the true* positions and δ_x, δ_y are the measurement noises.

- *vehicle depth* η_{1z} measured by the STS DTM depth sensor:
$$\eta_{1z}^{meas} = \eta_{1z} + \delta_z \tag{12}$$
where η_{1z}^{meas} and η_{1z} are the measured *and the true depths* and δ_z is the measurement noise.

Introducing the measurement vector $\boldsymbol{z} = \begin{pmatrix} \boldsymbol{\eta}_1^{measT} & \boldsymbol{\eta}_2^{measT} \end{pmatrix}^T$, the measurement equations can be summarized as follows:

$$\begin{aligned} \boldsymbol{z} &= \boldsymbol{h}(\boldsymbol{x}) + \boldsymbol{v}, \\ \boldsymbol{h}(\boldsymbol{x}) &= \begin{pmatrix} O_{3\times3} & O_{3\times3} & I_{3\times3} & O_{3\times3} \\ O_{3\times3} & O_{3\times3} & O_{3\times3} & I_{3\times3} \end{pmatrix} \boldsymbol{x}, \\ \boldsymbol{v} &= \begin{pmatrix} \delta_x & \delta_y & \delta_z & \boldsymbol{\delta}_{\eta 2}^T \end{pmatrix}^T. \end{aligned} \tag{13}$$

At each time step, the dimension of the measurement vector $\boldsymbol{z}$ can be different, depending on the available measurements (e.g. as concerns the GPS, the position information is available only when the vehicle is on surface). *Despite the different working frequencies of the various involved sensors, the correction step of the filter runs recursively at a desired constant rate equal to 10 Hz for the implemented filters. Furthermore, some sensor measurements could not always be available or could be corrupted. Consequently, in order to manage the variable size of the measurement vector due to the reasons above, the matrix describing the* $\boldsymbol{h}(\boldsymbol{x})$ *function in equation (13) is re-sized accordingly by eliminating the rows corresponding to the missing measurements for the particular instant.*
The sensors working frequencies are for sure important in the estimation process; generally speaking, the higher they are the better is the estimation result. The test case proposed in the paper is cautionary and stressful enough for the estimation algorithm, considering that the sensor set of our AUV is not too much expensive and composed of quite common sensors in the underwater field.

3.3. The propulsion system

The layout of the propulsion system of Typhoon class AUVs is shown in Fig. 5. Linear motions along longitudinal, lateral

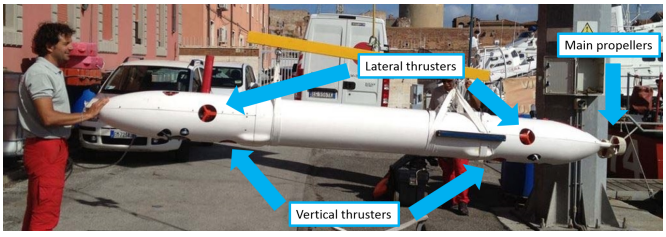

Figure 5: The propulsion system layout of the Typhoon AUV.

and vertical directions as well as pitch and yaw rotations are directly controlled by the propulsion system composed of two main propellers (longitudinal) and four thrusters (two vertical and two lateral) (see Fig. 6). Moreover, the longitudinal position of the accumulators (LiPo batteries), needed to power the vehicle, can be modified to better set the vehicle pitch.

3.3.1. Propulsion system modelling

The aim of this Section is to briefly describe the analytical model which relates the resultant forces and moments acting on the AUV $\boldsymbol{\tau}(\boldsymbol{\nu}, \boldsymbol{u})$ *(the term on the right side of Eq. (5)) to the vehicle speed* $\boldsymbol{\nu}$ *and to the rotational speed of the motors* $\boldsymbol{u}$

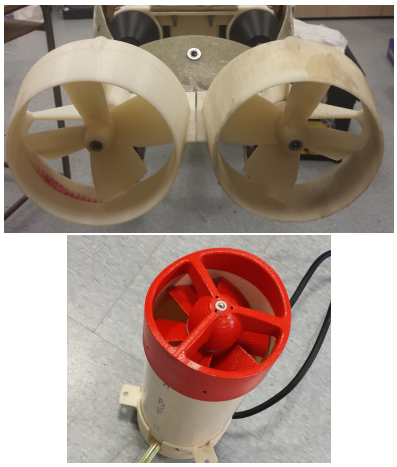

Figure 6: The propellers (above) and the thrusters (below) of the Typhoon AUV.

(which constitute the control inputs of the system). In particular, the analysis is focused on the generated motor force T_i (for the $i-th$ motor); the generated moments C_i can be, to a first approximation, neglected since a careful mechanical design of the AUV can greatly reduce their effect on the vehicle.
A necessary preliminary step is the determination of a law which expresses the thrust generated by a single propeller as a function of its rotational speed and of the advance velocity of the vehicle: $T_i = T_i(\boldsymbol{\nu}, u_i)$, where u_i is the $i-th$ of $\boldsymbol{u}$. Then, the resultant effect on the AUV is computed as a combination of the thrusts exerted by all the propellers of the vehicle. The motor characteristic $T_i = T_i(\boldsymbol{\nu}, u_i)$ can be found in the literature (tabulated or approximated through analytical expressions; see for example [16], [33]) and, usually, are highly nonlinear and non-differentiable functions. Consequently, they require particular attention when implemented in the navigation filter (the ability to cope with non-differentiable functions is indeed one of the strengths of the UKF).
At this step of the research activity, the authors have approximated the four-quadrant motor characteristic $T_i = T_i(\boldsymbol{\nu}, u_i)$ by means of the following function (see [2], [16], [33]):

$$T_i(\boldsymbol{\nu}, u_i) = sgn(u_i)\left(k{u_i}^2 - \frac{k|u_i|g\left(sgn(u_i)V_{a,i}\right)}{p}\right), \tag{14}$$

where $g(\cdot)$ is a piecewise function defined as

$$g(x) = \begin{cases} 0 & for\ x \leq 0 \\ x & for\ 0 < x \leq |u_i|p \\ |u_i|p & for\ x > |u_i|p \end{cases}. \tag{15}$$

and p is the propeller pitch. Eq. (14) describes, in an analytical way, the thrust T_i generated by a propeller, at a given rotational speed u_i, with advancing velocity $V_{a,i}$ (the velocity component along the motor rotation axis).
Finally, the advancing velocity $V_{a,i}$ of the i-th propeller of the AUV can be expressed as a function of $\boldsymbol{\nu}$ as follows:

$$V_{a,i} = \boldsymbol{n}_{mi}^{bT}\left[\boldsymbol{\nu}_1 + \boldsymbol{\nu}_2 \times \left(\boldsymbol{P}_{mi}^b - \boldsymbol{O}^b\right)\right], \tag{16}$$

where $\boldsymbol{P}_{mi}^b$ is the position of the i-th motor (expressed in the body frame), $\boldsymbol{n}_{mi}^b$ is the line of action of the i-th motor (expressed in the body frame) and $\times$ is the vector cross-product operator. Eq. 14 and Eq. 16 allow to get the required motor characteristic of the $i-th$ motor: $T_i = T_i(\boldsymbol{\nu}, u_i)$ by a simple substitution.
Once the thrust T_i for each propeller of the vehicle is known, the resulting vector of force and moment acting on the AUV can be computed. Let

$$\boldsymbol{U} = [T_1\ T_2\ \cdots T_i \cdots T_m]^T \in \mathbb{R}^m, \quad T_i = T_i(\boldsymbol{\nu}, u_i) \tag{17}$$

denote the vector collecting the thrusts exerted by the m propellers of the vehicle; then, the vector of force and moment acting on the vehicle $\boldsymbol{\tau}(\boldsymbol{\nu}, \boldsymbol{u})$ is computed following the linear model:

$$\boldsymbol{\tau}(\boldsymbol{\nu}, \boldsymbol{u}) = B\boldsymbol{U}(\boldsymbol{\nu}, \boldsymbol{u}), \quad \boldsymbol{u} = [u_1\ u_2\ \cdots\ u_m]^T. \tag{18}$$

Matrix B is constant and dependent on the vehicle geometry, and it is expressed as follows:

$$B = \begin{bmatrix} A_1 \\ A_2 \end{bmatrix}, \tag{19}$$

with

$$A_1 = \left[\boldsymbol{n}_{m1}^b \cdots \boldsymbol{n}_{mi}^b \cdots \boldsymbol{n}_{mm}^b\right] \tag{20}$$

$$A_2 = \left[\left(\boldsymbol{P}_{m1}^b - \boldsymbol{O}^b\right) \times \boldsymbol{n}_{m1}^b \cdots \left(\boldsymbol{P}_{mi}^b - \boldsymbol{O}^b\right) \times \boldsymbol{n}_{mi}^b \cdots \left(\boldsymbol{P}_{mm}^b - \boldsymbol{O}^b\right) \times \boldsymbol{n}_{mm}^b\right]. \tag{21}$$

3.4. The control system

The control system of Typhoon AUV is based on a classical feedback PID approach [19] working on all the controlled DOFs of the considered vehicle (longitudinal, lateral and vertical translations and yaw and pitch rotations):

$$\boldsymbol{\tau} = K_P\boldsymbol{e} + K_D\dot{\boldsymbol{e}} + K_I\int \boldsymbol{e}dt, \qquad \boldsymbol{\tau} = \boldsymbol{\tau}(\boldsymbol{\nu}, \boldsymbol{u}) = B\boldsymbol{U}(\boldsymbol{\nu}, \boldsymbol{u}) \tag{22}$$

where $\boldsymbol{\tau}$ are the desired control forces and torques acting on the vehicle (to be achieved through suitable control signals $\boldsymbol{u}$ of the vehicle motors, that is the motor rotation speed), $\boldsymbol{e}$ is the control error on all the vehicle DOFs (i. e. the difference between the desired $\boldsymbol{\eta}_d$ and the actual $\boldsymbol{\eta}$) and K_P, K_I, K_D are suitable (proportional, integral, derivative) gain matrices to be properly tuned so as to achieve the required control performance.

4. EKF-based navigation system

The complete system describing the AUV motion

$$\begin{aligned} \dot{\boldsymbol{x}} &= \boldsymbol{F}(\boldsymbol{x}, \boldsymbol{u}) + \boldsymbol{w} \\ \boldsymbol{z} &= \boldsymbol{h}(\boldsymbol{x}) + \boldsymbol{v} \end{aligned} \tag{23}$$

has been discretized by the Euler method with sampling interval $\Delta t = 0.01$s taking into account the different working frequen-

cies of the employed sensors:

$$\begin{aligned} \boldsymbol{x}_k &= \boldsymbol{f}(\boldsymbol{x}_{k-1}, \boldsymbol{u}_{k-1}) + \boldsymbol{w}_{k-1} = \\ &= \boldsymbol{x}_{k-1} + \Delta t\, \boldsymbol{F}(\boldsymbol{x}_{k-1}, \boldsymbol{u}_{k-1}) + \boldsymbol{w}_{k-1} \\ \boldsymbol{z}_k &= \boldsymbol{h}(\boldsymbol{x}_k) + \boldsymbol{v}_k. \end{aligned} \tag{24}$$

The standard navigation system used to estimate the vehicle dynamics is based on the classical EKF estimator (tested offline using the data provided by the Typhoon AUV) [11] [17] [36] [5] [6]:

$$\widehat{\boldsymbol{x}}_{k|k-1} = \boldsymbol{f}(\widehat{\boldsymbol{x}}_{k-1|k-1}, \boldsymbol{u}_{k-1}) \tag{25}$$

$$P_{k|k-1} = F_{k-1} P_{k-1|k-1} F_{k-1}^T + Q_{k-1} \tag{26}$$

$$F_{k-1} = \left.\frac{\partial \boldsymbol{f}}{\partial \boldsymbol{x}}\right|_{\widehat{\boldsymbol{x}}_{k-1|k-1}, \boldsymbol{u}_{k-1}} \tag{27}$$

$$\widehat{\boldsymbol{x}}_{k|k} = \widehat{\boldsymbol{x}}_{k|k-1} + K_k \boldsymbol{e}_k \tag{28}$$

$$P_{k|k} = (1 - K_k H_k)\, P_{k|k-1} \tag{29}$$

$$\boldsymbol{e}_k = \boldsymbol{z}_k - \boldsymbol{h}(\widehat{\boldsymbol{x}}_{k|k-1}) \tag{30}$$

$$H_k = \left.\frac{\partial \boldsymbol{h}}{\partial \boldsymbol{x}}\right|_{\widehat{\boldsymbol{x}}_{k|k-1}} \tag{31}$$

$$K_k = P_{k|k-1} H_k^T S_k^{-1} \tag{32}$$

$$S_k = H_k P_{k|k-1} H_k^T + R_k \tag{33}$$

where: $\boldsymbol{f}$ and $\boldsymbol{h}$ are state transition and observation functions; $\boldsymbol{x}$ and $\widehat{\boldsymbol{x}}$ are the system state and its estimate (the navigation outputs including all the required vehicle physical quantities in terms of position and orientation); P is the system state covariance matrix; $\boldsymbol{u}$ are the system inputs related to the motor control signals; $\boldsymbol{z}$ are the measurements provided by the set of sensors (IMU, pressure sensor and GPS during the surfaces); $\boldsymbol{w}$, $\boldsymbol{v}$, Q and R are the process and observation additive noises (both assumed zero mean Gaussian) and their covariances.

5. UKF-based navigation system

In this chapter, the UKF-based navigation algorithm will be described in detail. Clearly, the UKF estimator will be applied to the same discretized system shown in (24). *In Fig. 7 the logical scheme of the AUV navigation system is given; this scheme can help the reader to understand the connections between the controller, the vehicle dynamics and the proposed navigation filter.* UKF algorithm is able to deal directly with highly nonlinear and non-differentiable systems, such as the dynamic system under analysis, improving the accuracy of the estimation. The UKF is based on the Unscented Transform (UT), a derivative-free technique capable of providing a more accurate statistical characterization of a Random Variable (RV) undergoing a nonlinear transformation [23], [39]. In particular, the UT is a deterministic technique suited to provide mean and covariance of a given RV subjected to a nonlinear function given a minimal set of its samples. The pseudo-code of the UT is reported in Table 1. Taking into account mean $\boldsymbol{x}$ and associated covariance matrix P of a generic RV as well as a transformation function $g(\cdot)$, the UT proceeds as follows:

- generates $2n_x + 1$ samples $\mathcal{X} \in \mathbb{R}^{n_x \times (2n_x+1)}$, the so called σ-points, starting from the mean $\boldsymbol{x}$ with deviation given by the matrix square root Σ of P;
- propagates the σ-points through the transformation function $g(\cdot)$ resulting in $\mathcal{G} \in \mathbb{R}^{n_x \times (2n_x+1)}$;
- calculates the new transformed mean $\hat{\boldsymbol{x}}$ and associated covariance matrix P_{gg} as well as the cross-covariance matrix P_{xg} of the initial and transformed σ-points.

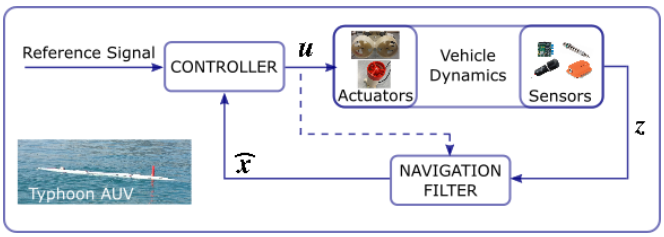

Figure 7: Logical flow diagram of the AUV navigation system.

Function `Unscented Transformation`($\boldsymbol{y}$, P, g)

▷ `Weights are calculated exploiting algorithm in Table 2`

1 $\Sigma \longleftarrow \sqrt{P}$

2 $\mathcal{Y} \longleftarrow \left[\boldsymbol{y} \dots \boldsymbol{y}\right] + \sqrt{c}\left[\boldsymbol{0}, \Sigma, -\Sigma\right]$

3 $\mathcal{G} \longleftarrow g(\mathcal{Y})$

4 $\hat{\boldsymbol{y}} \longleftarrow \mathcal{G} w_m$

5 $P_{gg} \longleftarrow \mathcal{G} W_c \mathcal{G}^T$

6 $P_{yg} \longleftarrow \mathcal{Y} W_c \mathcal{G}^T$

return $\hat{\boldsymbol{y}}$, P_{gg}, P_{xg}

end

Table 1: The Unscented Transformation algorithm

Function `Unscented Transformation Weights`(α, β, κ)

1 $\lambda \longleftarrow \alpha^2(n_x + \kappa) - n_x$

2 $w_m^{(0)} \longleftarrow \lambda\,(n_x + \lambda)^{-1}$

3 $w_c^{(0)} \longleftarrow \lambda\,(n_x + \lambda)^{-1} + (1 - \alpha^2 + \beta)$

4 $w_m^{(1,\dots,2n_x)}, w_c^{(1,\dots,2n_x)} \longleftarrow [2(n_x + \lambda)]^{-1}$

5 $\boldsymbol{w}_m = \left[w_m^{(0)}, \dots, w_m^{(2n_x)}\right]^T$, $\boldsymbol{w}_c = \left[w_c^{(0)}, \dots, w_c^{(2n_x)}\right]^T$

6 $W_c \longleftarrow (I - [\boldsymbol{w}_m \dots \boldsymbol{w}_m]) \times \mathrm{diag}\left(\boldsymbol{w}_c^{(0)} \dots \boldsymbol{w}_c^{(2n)}\right) \times (I - [\boldsymbol{w}_m \dots \boldsymbol{w}_m])^T$

7 $c \longleftarrow \alpha^2(n_x + \kappa)$

return c, $\boldsymbol{w}_m$, W_c

end

Table 2: The Unscented Transformation weights algorithm

It is worth pointing out that the weights c, w_m and W_c are calculated exploiting the algorithm in Table 2, given three param-

eters α, β and κ. Moment matching properties and performance improvements are discussed in [23], [39] resorting to specific values of α, β and κ. It is common practice to set these three parameters as constants computing the weights at the beginning of the estimation process. I.e. UKF is usually tuned through a heuristic approach. If in the considered system the aleatory variables are Gaussian, the optimal values of the tuning parameters have been given in literature [23]. The UT can be applied in the KF recursion allowing to adopt a nonlinear recursive estimator known as UKF [23]. The pseudo-code of the UKF is shown in Table 3. Due to its well-known benefits [23], the UKF

Function `Unscented Kalman Filter`$(\hat{\boldsymbol{x}}_{k-1|k-1}, P_{k-1|k-1}, f(\cdot), h(\cdot))$

▷ `Prediction`

1 $\hat{\boldsymbol{x}}_{k|k-1}, P_{k|k-1} \longleftarrow \mathtt{UT}(\hat{\boldsymbol{x}}_{k-1|k-1}, P_{k-1|k-1}, f(\cdot))$

2 $P_{k|k-1} \longleftarrow P_{k|k-1} + Q$

▷ `Correction`

3 $\hat{\boldsymbol{z}}_{k|k-1}, S_k, C_k \longleftarrow \mathtt{UT}(\hat{\boldsymbol{x}}_{k|k-1}, P_{k|k-1}, h(\cdot))$

4 $S_k \longleftarrow S_k + R$

5 $\hat{\boldsymbol{x}}_{k|k} \longleftarrow \hat{\boldsymbol{x}}_{k|k-1} + C_k S_k^{-1} (\boldsymbol{z}_k - \hat{\boldsymbol{z}}_{k|k-1})$

6 $P_{k|k} \longleftarrow P_{k|k-1} - C_k S_k^{-1} C_k^T$

end

Table 3: The Unscented Kalman Filter algorithm

is adopted as the nonlinear recursive estimator of the AUV dynamical system.

6. Experimental validation of the navigation system

In this chapter, the navigation system described in section 2 will be validated offline for both classical EKF-based and UKF-based implementations throughout experimental data. The experimental data were collected during the sea tests performed in La Spezia (Italy) in September 2013 (see Fig. 1) in the framework of the NATO CommsNet13 experimental campaign. The tests have been organized and scientifically led by the NATO Science and Technology Organization Centre for Maritime Research and Experimentation (NATO STO CMRE).

6.1. The experimental campaign

The CommsNet13 experiment took place in September 2013 in the La Spezia Gulf, North Tyrrhenian Sea, with the support of NATO Research Vessel Alliance. The experiment was scientifically led by the NATO Science and Technology Organization Centre for Maritime Research and Experimentation (NATO STO CMRE, formerly NURC) and included, among its objectives, the testing of several acoustic communication and localization systems using underwater networks. In fact, in the area, the CMRE has a permanent testbed for underwater networking and communication purposes (LOON - Littoral Ocean Observatory Network). During CommsNet13, the LOON installation consisted of 4 EvoLogics modems, placed on the seabed and cable-connected to the shore (they could be continuously operated and monitored). LOON has been exploited to evaluate the on-board USBL systems of the AUVs.
The Typhoon class TifTu took part to the experimentation at sea. TifTu was equipped with an EvoLogics acoustic modem/USBL head and navigated within the fixed nodes acoustic network deployed by the CMRE. The LOON modems are compatible with those installed on-board the Typhoon, so that the vehicle could use its USBL modem to estimate its relative position with respect to the fixed LOON installation: this allows the comparison between inertial navigation and acoustic self-localization as ground truth.
Throughout the experiments, TifTu autonomously traveled in dead reckoning and was equipped with the IMU, the pressure sensor for the depth, the GPS sensor (used during the periodic and dedicated resurfacing: one every 2.5 minutes) and the USBL unit (used only as ground truth). TifTu traveled along a triangle-shaped path on the LOON area. The reference path for the underwater mission was defined by three waypoints respectively called Janus1, M2 (position of the second one of the four LOON modems) and Typhoon1. The length of the path side was about 190 $[m]$) and the mission was performed at the depth of about 4.5 $[m]$ (see Fig. 8). The TifTu AUV navigated underwater for a total of 1150 $[s]$ at a speed of 0.6 $[m/s]$. The

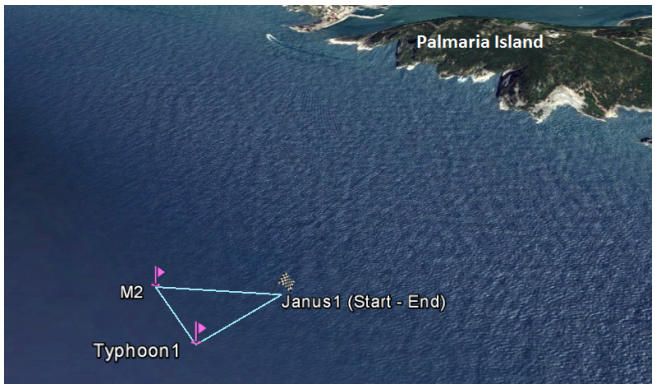

Figure 8: Layout of the autonomous mission: triangle-shaped path with vertices placed in the waypoints Janus1, M2 and Typhoon1.

aim of the mission is twofold: 1) understand whether or not the filters are capable of reconstructing the shape of the desired trajectory during a navigation task; 2) to understand the position drift error generated during the filtering process (using the USBL as reference to evaluate the filter accuracy). The drift error is due to the fact that the available measurements provided by the exploited sensors (IMU, pressure sensor for the depth and GPS only during the resurfacing) do not directly provide the position of the AUV.

6.2. The mission

In this subsection, the EKF-based and the UKF-based navigation systems will be compared during an underwater mission. Fig. 9 and Fig. 10 show the estimated Cartesian position coordinates η_{1x}^{EKF}, η_{1y}^{EKF} and η_{1x}^{UKF}, η_{1y}^{UKF} provided by both navigation system implementations. The GPS fixes η_{1x}^{GPS}, η_{1y}^{GPS} (dur-

ing the resurfacing) and the USBL fixes η_{1x}^{USBL}, η_{1y}^{USBL} are also provided for the sake of comparison. Tab. 4 summarizes the USBL fixes η_{1x}^{USBL}, η_{1y}^{USBL} (used as reference), the estimation error $\left\|\boldsymbol{\eta}_1^{EKF} - \boldsymbol{\eta}_1^{USBL}\right\|$ affecting $\boldsymbol{\eta}_1^{EKF}$ and the estimation error $\left\|\boldsymbol{\eta}_1^{UKF} - \boldsymbol{\eta}_1^{USBL}\right\|$ affecting $\boldsymbol{\eta}_1^{UKF}$.

The classical EKF-based navigation system, representing the standard for the underwater navigation, shows poorer performance compared to the UKF-based one during the underwater mission. The achieved results seem to be encouraging, and the use of the UKF filter turns out to be quite promising since the UKF estimations are often better than the EKF ones. This good behaviour of the proposed UKF filter is confirmed also by the other tests performed in La Spezia (not reported in the paper for reason of brevity).

For the sake of completeness the measured and filtered vehicle orientations $\boldsymbol{\eta}_2^{meas}$, $\boldsymbol{\eta}_2^{EKF}$, $\boldsymbol{\eta}_2^{UKF}$ and depths η_{1z}^{meas}, η_{1z}^{EKF}, η_{1z}^{UKF} are reported in Figs. 11-14: these figures show a good matching with the filtered quantities. The disturbances and noise affecting the behaviour of vehicle orientations and depths are not due to the navigation systems analyzed offline in this paper, but are caused by the simple navigation system of the real vehicle (pure dead reckoning) and to its simple control system (a PID [19]).

7. Conclusions and further developments

In this paper, the authors presented a navigation system for AUVs. The system exploits a sensor suite consisting of an Inertial Measurement Unit (IMU), a Pressure Sensor (PS) for the depth and a GPS (used only during periodic and dedicated resurfacing), and relies either on the Extended Kalman Filter (EKF) or the Unscented Kalman Filter (UKF) for AUV state estimation. Both EKF and UKF navigation algorithms have been experimentally evaluated offline by means of sea navigation tests performed in La Spezia (Italy) with the Typhoon AUV navigating in dead reckoning during the NATO CommsNet13 experiment. Experimental results exhibited a satisfactory localization accuracy for both EKF and UKF, the latter being more accurate than the former.

Some important further developments are scheduled for the near future. First, the UKF-based navigation system will be implemented on-board and tested online on the Typhoon AUV. In fact, thanks to the encouraging results obtained, online implementation will follow soon the preliminary offline validation procedure here presented. This way, the performance of the navigation system will be carefully investigated in different critical scenarios. Moreover, the robustness of the proposed algorithm will be evaluated during the next steps of this research activity, performing dedicated tests with different sensors and under different environmental disturbances. Finally, the AUV modelling will be further improved and more advanced control techniques (including nonlinear and robust control) will be tested. There are many advanced nonlinear control methods, also suitable for AUVs, and the authors are evaluating them to be tested during the next experimental campaigns: in particular, a Sliding Mode Control is currently under analysis.

8. Acknowledgments

This work has been supported by the Italian THESAURUS project (funded by PAR FAS Regione Toscana, Linea di Azione 1.1.a.3) and by the European ARROWS project (this project has received funding from the European Union's Seventh Framework Programme for Research technological development and demonstration, under grant agreement no. 308724). The authors would like to thank the NATO Science and Technology Organization Centre for Maritime Research and Experimentation (NATO STO CMRE) (La Spezia, Italy) for providing facilities and support during all the research activity. A special thanks also goes to the *Comune di San Miniato* (Pisa, Italy) and the rowing club *Canottieri San Miniato* for their precious help during the experimental campaigns in Tuscany. Finally, the authors would like to thank the colleagues of the MDM Lab of the University of Florence for the theoretical and experimental work during the whole research projects and Alessio Cuccoli who worked on this topic during his Master Thesis.

References

[1] B. Allotta. http://www.arrowsproject.eu. *Official Site of the European ARROWS Project*, 2015.

[2] B. Allotta, F. Bartolini, R. Costanzi, N. Monni, L. Pugi, A. Ridolfi, and J. Gelli. Preliminary design and fast prototyping of an autonomous underwater vehicle propulsion system. *Proceedings of the Institution of Mechanical Engineers - Part M, Journal of Engineering for the Maritime Environment*, 229(3):248–272, 2015.

[3] B. Allotta and A. Caiti. http://thesaurus.isti.cnr.it. *Official Site of the Italian THESAURUS Project*, 2013.

[4] B. Allotta, R. Costanzi, F. Fanelli, N. Monni, and A. Ridolfi. Single axis fog aided attitude estimation algorithm for mobile robots. *Mechatronics*, 30:158–173, 2015.

[5] B. Allotta, R. Costanzi, E. Meli, L. Pugi, A. Ridolfi, and G. Vettori. Cooperative localization of a team of auvs by a tetrahedral configuration. *Robotics and Autonomous Systems*, 62:1228–1237, 2014.

[6] B. Allotta, R. Costanzi, N. Monni, L. Pugi, A. Ridolfi, and G. Vettori. Design and simulation of an autonomous underwater vehicle. In *Proceedings of the European Congress on Computational Methods in Applied Sciences and Engineering, ECCOMAS 2012*, Vienna, Austria, 2012.

[7] B. Allotta, R. Costanzi, A. Ridolfi, and et al. The arrows project: adapting and developing robotics technologies for underwater archaeology. In *Proceedings of the IFAC Workshop on Navigation Guidance and Control of Underwater Vehicles (NGCUV 2015)*, Girona, Spain, 2015.

[8] J. Alves, J. Potter, G. Zappa, P. Guerrini, and R. Been. A testbed for collaborative development of underwater communications and networking. In *Military Communications Conference 2012, MILCOM*, Orlando, FL, October-November 2012.

[9] F. Arrichiello, G. Antonelli, A. P. Aguiar, and A. Pascoal. Observability metric for the relative localization of auvs based on range and depth measurements: Theory and experiments. In *IEEE/RSJ International Conference on Intelligent Robots and Systems (IROS)*, San Francisco, CA, USA, 2011.

[10] A. Bahr, J.J. Leonard, and M.F. Fallon. Cooperative localization for autonomous underwater vehicles. *The International Journal Robotics Research*, 28:714–728, 2009.

[11] Y. Bar-Shalom, X. Rong Li, and T. Kirubarajan, editors. *Estimation with Applications to Tracking and Navigation*. Wiley and Sons, New York, NY, USA, 2001.

[12] M. Barisic, A. Vasilijevic, and D. Nad. Sigma-point unscented kalman filter used for auv navigation. In *Proceedings of the 20th Mediterranean Conference on Control and Automation*, Barcelona, Spain, 2012.

[13] P. Batista, C. Silvestre, and P. Oliveira. Single range aided navigation and source localization: observability and filter design. *Systems and Control Letters*, 60:665–673, 2011.

[14] M. Breivik and T. I. Fossen. Guidance-based path following for autonomous underwater vehicles. In *Proceedings of the IEEE OCEANS 2005*, Washington D.C.,USA, 2005.

[15] A. Caiti, V. Calabrò, T. Fabbri, D. Fenucci, and A. Munafò. Underwater communication and distributed localization of auv teams. In *Proceedings of IEEE OCEANS 2013*, San Diego, CA, USA, 2013.

[16] J. Carlton, editor. *Marine propellers and Propulsion, 2nd edition*. Elsevier Butterworth-Heinemann, Oxford, UK, 2007.

[17] G. Evensen, editor. *Data Assimilation*. Springer Verlag, Heidelberg, Germany, 2009.

[18] O. Fjellstad and T. I. Fossen. Position and attitude tracking of auv's: A quaternion feedback approach. *IEEE Journal of Oceanic Engineering*, 19:512–518, 1994.

[19] T.I. Fossen. *Guidance and Control of Ocean Vehicles*. John Wiley and Sons, London, UK, 1994.

[20] T.I. Fossen and O.E. Fjellstad. Nonlinear modelling of marine vehicles in 6 degrees of freedom. *Journal of Mathematical Modelling of Systems*, 1(1), 1995.

[21] D. Gebre-Egziabhern. Design and performance analysis of a low-cost aided dead reckoning navigator. In *Ph.D. Thesis*, Standford University, CA, USA, 2004.

[22] C. Hajiyev, M. Ata, M. Dinc, and H.E. Soken. Fault tolerant estimation of autonomous underwater vehicle dynamics via robust ukf. In *Proceedings of the 13th International Carpathian Control Conference*, 2012.

[23] S. Julier and J. Uhlmann. Unscented filtering and nonlinear estimaion. *Proceedings of the IEEE*, 92:401–422, 2004.

[24] R. E. Kalman. A new approach to linear filtering and prediction problems. *Journal of Basic Engineering*, 82:35–45, 1960.

[25] M. Karimi, M. Bozorg, and A.R. Khayatian. A comparison of dvl/ins fusion by ukf and ekf to localize an autonomous underwater vehicle. In *Proceedings of the First RSI/ISM International Conference on Robotics and Mechatronics, ICRoM 2013*, Tehran, Iran, 2013.

[26] M.B. Larsen. Synthetic long baseline navigation of underwater vehicles. In *Proceedings of MTS/IEEE OCEANS 2000*, Providence, RI, USA, 2000.

[27] D. Loebis, R. Sutton, J. Chudley, and W. Naeem. Adaptive tuning of a kalman filter via fuzzy logic for an intelligent auv navigation system. *Control Engineering Practice*, 12:1531–1539, 2004.

[28] R.E. Mahony, T. Hamel, and J.M. Pflimlin. Nonlinear complementary filters on the special orthogonal group. *IEEE Trans. on Automatic Control*, 53:1203–1218, 2008.

[29] D.B. Marco and A.J. Healey. Command, control, and navigation experimental results with the nps aries auv. *IEEE Journal of Oceanic Engineering*, 26:466–476, 2001.

[30] G.E. Packard, A. Kukulya, T. Austin, M. Dennett, R. Littlefield, G. Packard, M. Purcell, R. Stokey, and G. Skomal. Continuous autonomous tracking and imaging of white sharks and basking sharks using a remus-100 auv. In *Proceedings of the IEEE OCEANS 2013*, San Diego, CA, USA, 2013.

[31] G. Parlangeli, P. Pedone, and G. Indiveri. Relative pose observability analysis for 3d nonholonomic vehicles based on range measurements only. In *Proceedings of the 9th IFAC Conference on Manoeuvring and Control of Marine Craft*, Arenzano, Italy, 2012.

[32] C. Petres, Y. Pailhas, P. Patron, Y. Petillot, J. Evans, and D. Lane. Path planning for autonomous underwater vehicles. *IEEE Transactions on Robotics*, 23:331–341, 2007.

[33] L. Pivano, T. A. Johansen, and Ø. N. Smogeli. A four-quadrant thrust estimation scheme for marine propellers: Theory and experiments. *Control Systems Technology, IEEE Transactions on*, 10.1109/TCST.2008.922602, 2009.

[34] P. Rigby, O. Pizarro, and S.B. Williams. Towards geo-referenced auv navigation through fusion of usbl and dvl measurements. In *Proceedings of MTS/IEEE OCEANS 2006*, Boston, MA, USA, 2006.

[35] B. Ristic, S. Arulampalam, and N. Gordon, editors. *Beyond the Kalman Filter*. Artech House Publishers, Boston, MA, USA, 2004.

[36] A. H. Sayed, editor. *Adaptive Filters*. Wiley and Sons, Hoboken, NJ, USA, 2009.

[37] S. Singh, M. Grund, B. Bingham, R. Eustice, H. Singh, and L. Freitag. Underwater acoustic navigation with the whoi micro-modem. In *Proceedings MTS/IEEE Conference and Exhibition OCEANS 2006*, Boston, MA, USA, 2006.

[38] R.P. Stokey, A. Roup, C. von Alt, B. Allen, N. Forrester, T. Austin, R. Goldsborough, M. Purcell, F. Jaffre, G. Packard, and A. Kukulya. Development of the remus 600 autonomous underwater vehicle. In *Proceedings of the IEEE OCEANS 2005*, Washington D.C.,USA, 2005.

[39] E. A. Wan and R. Van Der Merwe. *The Unscented Kalman Flter*. S. Haykin Edition, New York, NY, USA, 2001.

[40] X. Yun, E.R. Bachmann, R.B. McGhee, R.H. Whalen, R.L. Roberts, R.G. Knapp, A.J. Healey, and M.J. Zyda. Testing and evaluation of an integrated gps/ins system for small auv navigation. *IEEE Journal of Oceanic Engineering*, 24:396–404, 1999.

[41] X. Yun, E.R. Bachmann, R.B. McGhee, R.H. Whalen, R.L. Roberts, R.G. Knapp, A.J. Healey, and M.J. Zyda. Testing and evaluation of an integrated gps/ins system for small auv navigation. *IEEE Journal of Oceanic Engineering*, 24:396–404, 1999.

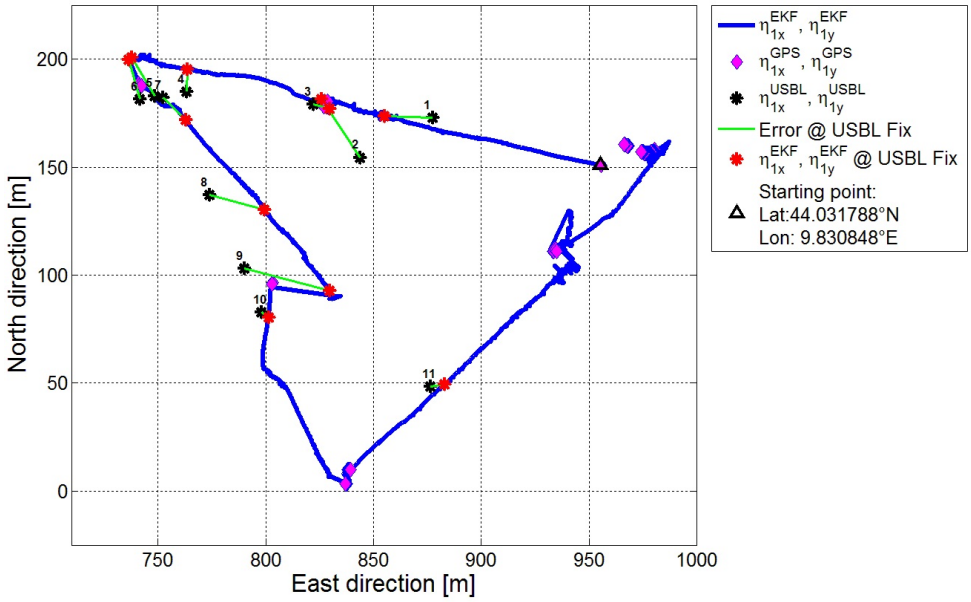

Figure 9: AUV trajectory estimated by the classical EKF-based navigation system along with the GPS and USBL fixes (the origin coordinates are: 44.03042984 ^oN, 9.81893253^oE).

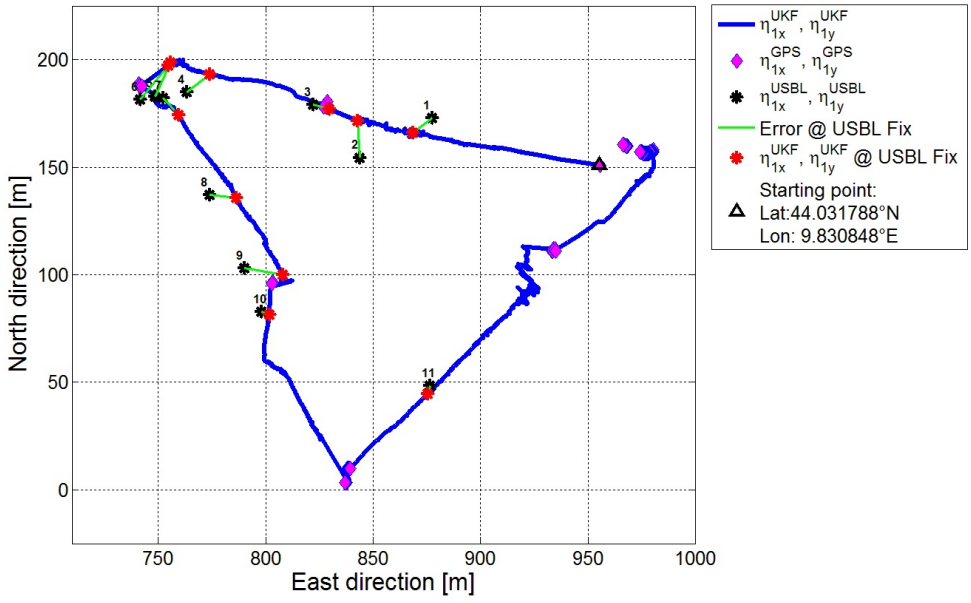

Figure 10: AUV trajectory estimated by the UKF-based navigation system along with the GPS and USBL fixes (the origin coordinates are: 44.03042984 ^oN, 9.81893253^oE).

Table 4: USBL fixes (η_{1x}^{USBL}, η_{1y}^{USBL}) and errors affecting $\boldsymbol{\eta}_1^{EKF}$ and $\boldsymbol{\eta}_1^{UKF}$ with respect to the USBL fixes.

Fix	η_{1x}^{USBL}	η_{1y}^{USBL}	Error on $\boldsymbol{\eta}_1^{EKF}$ ($[m]$)	Error on $\boldsymbol{\eta}_1^{UKF}$ ($[m]$)
USBL fix N^o1	44.031985 ^oN	9.829877 ^oE	22.3	11.1
USBL fix N^o2	44.031820 ^oN	9.829461 ^oE	32.4	17.0
USBL fix N^o3	44.032042 ^oN	9.829189 ^oE	7.8	7.7
USBL fix N^o4	44.032093 ^oN	9.828454 ^oE	10.4	13.6
USBL fix N^o5	44.032076 ^oN	9.828269 ^oE	20.7	17.3
USBL fix N^o6	44.032063 ^oN	9.828184 ^oE	18.9	20.8
USBL fix N^o7	44.032069 ^oN	9.828319 ^oE	14.8	10.6
USBL fix N^o8	44.031664 ^oN	9.828586 ^oE	26.4	12.4
USBL fix N^o9	44.031357 ^oN	9.828791 ^oE	40.3	18.1
USBL fix N^o10	44.031175 ^oN	9.828890 ^oE	4.0	3.8
USBL fix N^o11	44.030865 ^oN	9.829867 ^oE	6.6	4.0

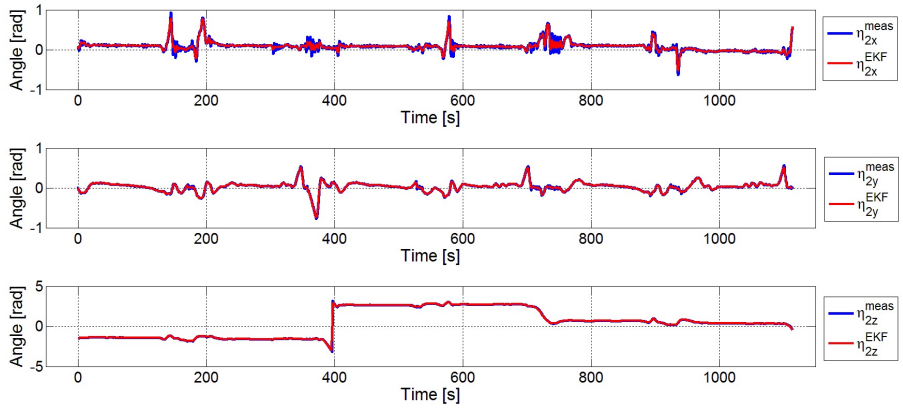

Figure 11: Comparison between $\boldsymbol{\eta}_2^{meas}$ and $\boldsymbol{\eta}_2^{EKF}$.

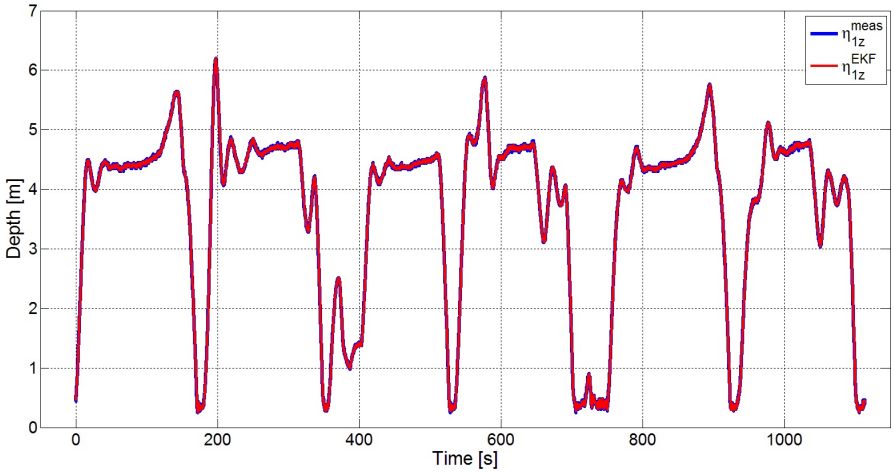

Figure 12: Comparison between η_{1z}^{meas} and η_{1z}^{EKF}.

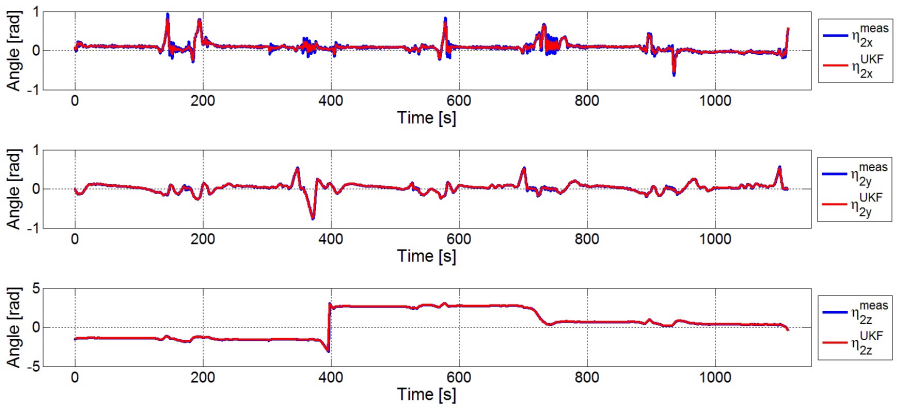

Figure 13: Comparison between $\boldsymbol{\eta}_2^{meas}$ and $\boldsymbol{\eta}_2^{UKF}$.

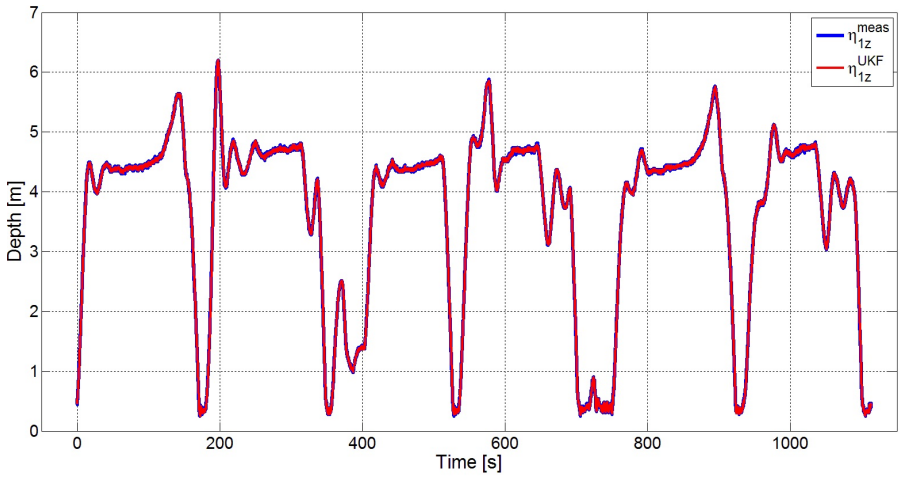

Figure 14: Comparison between $\eta_{1_z}^{meas}$ and $\eta_{1_z}^{UKF}$.